J Sci Comput (2016) 66:598–624
DOI 10.1007/s10915-015-0041-4

Finite Difference Hermite WENO Schemes for Conservation Laws, II: An Alternative Approach

Hongxia Liu[1] · **Jianxian Qiu**[2]

Received: 10 July 2014 / Revised: 16 April 2015 / Accepted: 2 May 2015 /
Published online: 10 May 2015

Abstract In Liu and Qiu (J Sci Comput 63:548–572, 2015), we presented a class of finite difference Hermite weighted essentially non-oscillatory (HWENO) schemes for conservation laws, in which the reconstruction of fluxes is based on the usual practice of reconstructing the flux functions. In this follow-up paper, we present an alternative formulation to reconstruct the numerical fluxes, in which we first use the solution and its derivatives directly to interpolate point values at interfaces of computational cells, then we put the point values at interface of cell in building block to generate numerical fluxes. The building block can be arbitrary monotone fluxes. Comparing with Liu and Qiu (2015), one major advantage is that arbitrary monotone fluxes can be used in this framework, while in Liu and Qiu (2015) the traditional practice of reconstructing flux functions can be applied only to smooth flux splitting. Furthermore, these new schemes still keep the effectively narrower stencil of HWENO schemes in the process of reconstruction. Numerical results for both one and two dimensional equations including Euler equations of compressible gas dynamics are provided to demonstrate the good performance of the methods.

Keywords HWENO schemes · Hermite interpolation · Finite difference method · Construction of polynomial · Hyperbolic conservation laws

Research was supported by NSFC Grants 91230110, 11328104, ISTCP of China Grant No. 2010DFR00700.

✉ Jianxian Qiu
jxqiu@xmu.edu.cn

Hongxia Liu
hx_ryu@163.com

1 School of Mathematical Sciences, Xiamen University, Xiamen 361005, Fujian, People's Republic of China

2 School of Mathematical Sciences and Fujian Provincial Key Laboratory of Mathematical Modeling and High-Performance Scientific Computing, Xiamen University, Xiamen 361005, Fujian, People's Republic of China

1 Introduction

In the recent decades, high resolution methods for hyperbolic systems of conservation laws have been extensively studied. Especially, HWENO schemes as new high order accurate numerical methods were developed for solving hyperbolic conservation laws. HWENO schemes which were first introduced by Qiu and Shu [12] in the form of finite volume version, and were applied as limiters for the Runge–Kutta discontinuous Galerkin (RKDG) methods for solving one-dimensional conservation laws. The schemes were extended to two-dimensional cases in [14,25]. Then the HWENO methods were applied to solve Hamilton-Jacobi equations in [15] and computational acoustics in [2]. HWENO methodology is designed based on the successful WENO schemes [1,6,8,11,16,17,19,20]. Mentioning WENO schemes, they are quite popular as high order numerical method for solving hyperbolic partial differential equations (PDEs). The first WENO schemes were introduced in 1994 by Liu, Osher and Chan in their pioneering paper [11], in which the third accurate order finite volume WENO in one space dimension was constructed. In 1996, Jiang and Shu [8] provided a general framework to design arbitrary accurate order finite difference WENO schemes, which are more efficient for multidimensional calculations. Very high order WENO schemes (seventh to eleventh order) are documented in [1]. For a detailed review of WENO schemes, we refer to the lecture notes [17,18].

However, in spite of the vast field application of WENO schemes, the classical WENO schemes still have deficiencies: due to the width of their numerical stencil, the extension to non-Cartesian meshes is somewhat cumbersome; moreover, a wide stencil is not optimum either in terms of an accurate treatment of weak fluctuations, or concerning the imposition of boundary conditions. Considering those limits, a possibility is to introduce more information of the numerical solution in the neighborhood of any given cell. HWENO schemes, using the Hermite interpolation, following the original WENO philosophy, the solution and its first derivative are evolved in time and used into the polynomial reconstruction. That is to say, HWENO schemes can obtain the higher accuracy while use relatively less points. Meanwhile, the HWENO scheme also has a disadvantage, for the same number of grid points, it requires more computer memory than the regular WENO scheme because of the auxiliary variables (or derivative equations) which were introduced.

On the other hand, in most of the high order finite difference schemes, for example, the high order finite difference ENO [20], WENO [1,8,18] and HWENO schemes [10], the reconstruction of fluxes is based on the usual practice of reconstructing the flux functions which was based on the procedure presented by Shu and Osher [20], because the procedure is clean and easy to implement. However, in order to achieve nonlinear stability and incorporate upwinding into the schemes, the numerical flux with finite difference in flux formulation has certain limits in its mathematical forms—satisfying the forms of flux splitting. The alternative approach to construct numerical fluxes in high order conservative finite difference schemes were developed in [19], in which the ENO interpolation [3–5] of the solution and its derivatives are used to directly construct the numerical flux which involves the interpolations directly on the point values of the solution u_i, v_i (and w_i) rather than on the flux values. Recently, in [9], Jiang, Shu and Zhang also developed the WENO schemes with Lax–Wendroff time discretization for conservation laws, the reconstruction of numerical fluxes were also based on the approach presented in [19], which overcome the defects the above stated the traditional method, like in [10]. Even though this approach is more expensive than the standard one, the major advantage is that arbitrary monotone fluxes can be used in this

framework, while the traditional practice of reconstructing flux functions can be applied only to smooth flux splitting, as pointed out in [9].

In [10], we presented a class of finite difference Hermite weighted essentially non-oscillatory (HWENO) schemes for conservation laws, in which the reconstruction of fluxes is based on the usual practice of reconstructing the flux functions. In view of this, in this subsequent paper, we continues studying the conservative finite difference HWENO methods but using the alternative formulation to solve the hyperbolic equations

$$\begin{cases} u_t + \nabla \cdot f(u) = 0, \\ u(x,0) = u_0(x) \end{cases} \tag{1.1}$$

where $x = (x_1, \ldots, x_d)$ are d-spatial variables.

In this follow-up paper, we present an alternative formulation to reconstruct the numerical fluxes, in which we first use the solution and its derivatives directly to interpolate point values at interfaces of computational cells, then we put the point values at interface of cell in building block to generate numerical fluxes. The building block can be arbitrary monotone fluxes. Comparing with [10], one major advantage is that arbitrary monotone fluxes can be used in this framework, while in [10] the traditional practice of reconstructing flux functions can be applied only to smooth flux splitting. The second advantage is that the new schemes still keep the the effectively narrower stencil of HWENO schemes in the process of reconstruction.

The paper is organized as follows. In next section we describe in detail the construction and implementation of the fifth order HWENO schemes, with Runge–Kutta time discretization, for one dimension scalar and system equations of (1.1). We present the fourth HWENO in two dimensional case in Sect. 3. In Sect. 4, extensive numerical results are given to demonstrate the behavior of this method, and some concluding remarks are given in the final section.

2 The Fifth Order HWENO Schemes for One Dimensional Conservation Laws

In this section, we will describe implementation procedure for a finite difference version of HWENO to solve hyperbolic conservation laws. We first discuss one dimensional scalar conservation laws of (1.1). We will define the following notation for our mesh $I_i = [x_{i-\frac{1}{2}}, x_{i+\frac{1}{2}}]$, $x_i = \frac{1}{2}(x_{i-\frac{1}{2}} + x_{i+\frac{1}{2}})$, $i = 1, \ldots, N$, where $x_{i+1/2} = x_i + \Delta x/2$ and $\Delta x = x_{i+1} - x_i$, which is assumed a uniform spatial mesh for simplicity.

We introduce a new function $v = u_x$, the system (1.1) can be written a coupled hyperbolic system:

$$\begin{cases} u_t + f(u)_x = 0, \quad u(x,0) = u_0(x), \\ v_t + h(u,v)_x = 0, \quad v(x,0) = v_0(x), \end{cases} \tag{2.1}$$

where $h(u,v) = f'(u)u_x = f'(u)v$. We can solve (2.1) directly using a conservation approximation to the spatial derivatives:

$$\begin{cases} \frac{du_i(t)}{dt} = -\frac{1}{\Delta x}(\hat{f}_{i+1/2} - \hat{f}_{i-1/2}) \\ \frac{dv_i(t)}{dt} = -\frac{1}{\Delta x}(\hat{h}_{i+1/2} - \hat{h}_{i-1/2}) \end{cases} \tag{2.2}$$

where $u_i(t)$, $v_i(t)$ are the numerical approximation to the nodal value $u(x_i,t)$ and $v(x_i,t)$ of the solution to (2.1) in a uniform grid. The numerical fluxes $\hat{f}_{i+\frac{1}{2}}$ and $\hat{h}_{i+\frac{1}{2}}$ are required to be a Lipschitz continuous function of several neighboring values u_i and v_i and also to be consistent with the physical fluxes $f(u)$ and $h(u,v)$.

In [10], the reconstruction of fluxes for HWENO schemes is based on the usual practice of reconstructing the flux functions [8,20], in this paper we will use an alternative approach to construct numerical fluxes for high order conservative finite difference schemes based on the procedure of [19].

If the numerical fluxes $\hat{f}_{i+\frac{1}{2}}$ and $\hat{h}_{i+\frac{1}{2}}$ are designed such that:

$$\begin{cases} \frac{1}{\Delta x}\left(\hat{f}_{i+\frac{1}{2}} - \hat{f}_{i-\frac{1}{2}}\right) = f(u)_x|_{x=x_i} + O(\Delta x^r) \\ \frac{1}{\Delta x}\left(\hat{h}_{i+\frac{1}{2}} - \hat{h}_{i-\frac{1}{2}}\right) = h(u,v)_x|_{x=x_i} + O(\Delta x^{r-1}) \end{cases} \tag{2.3}$$

then the conservative difference scheme (2.2) will be the r-th order approximation to Eq. (2.1), when the solution is smooth. Following the procedure of [19], we divide the fluxes $\hat{f}_{i+\frac{1}{2}}$ and $\hat{h}_{i+\frac{1}{2}}$ into two parts, respectively,

$$\begin{cases} \hat{f}_{i+\frac{1}{2}} = \hat{f}^L_{i+\frac{1}{2}} + \hat{f}^H_{i+\frac{1}{2}} \\ \hat{h}_{i+\frac{1}{2}} = \hat{h}^L_{i+\frac{1}{2}} + \hat{h}^H_{i+\frac{1}{2}} \end{cases} \tag{2.4}$$

where numerical flux $\hat{f}^L_{i+\frac{1}{2}} = \hat{f}^L(u^-_{i+\frac{1}{2}}, u^+_{i+\frac{1}{2}})$ and $\hat{h}^L_{i+\frac{1}{2}} = \hat{h}^L(u^-_{i+\frac{1}{2}}, u^+_{i+\frac{1}{2}}, v^-_{i+\frac{1}{2}}, v^+_{i+\frac{1}{2}})$ can be arbitrary fluxes, $u^\pm_{i+\frac{1}{2}}$ and $v^\pm_{i+\frac{1}{2}}$ are approximations to u and v at $x_{i+\frac{1}{2}}$, respectively. As in [19], we will adopt the following fluxes in this paper:

$$\hat{f}^L_{i+\frac{1}{2}} = \hat{f}^{LF}_{i+\frac{1}{2}} = \frac{1}{2}\left(f\left(u^+_{i+\frac{1}{2}}\right) + f\left(u^-_{i+\frac{1}{2}}\right)\right) - \frac{\alpha}{2}\left(u^+_{i+\frac{1}{2}} - u^-_{i+\frac{1}{2}}\right), \tag{2.5}$$

$$\hat{f}^H_{i+\frac{1}{2}} \approx a_2\Delta x^2\left(\frac{\partial^2 f}{\partial x^2}\right)_{i+\frac{1}{2}} + a_4\Delta x^4\left(\frac{\partial^4 f}{\partial x^4}\right)_{i+\frac{1}{2}}, \tag{2.6}$$

$$\hat{h}^L_{i+\frac{1}{2}} = \hat{h}^{LF}_{i+\frac{1}{2}} = \frac{1}{2}\left(h\left(u^-_{i+\frac{1}{2}}, v^-_{i+\frac{1}{2}}\right) + h\left(u^+_{i+\frac{1}{2}}, v^+_{i+\frac{1}{2}}\right)\right) - \frac{\alpha}{2}\left(v^+_{i+\frac{1}{2}} - v^-_{i+\frac{1}{2}}\right), \tag{2.7}$$

$$\hat{h}^H_{i+\frac{1}{2}} \approx a_2\Delta x^2\left(\frac{\partial^2 h}{\partial x^2}\right)_{i+\frac{1}{2}} + a_4\Delta x^4\left(\frac{\partial^4 h}{\partial x^4}\right)_{i+\frac{1}{2}}, \tag{2.8}$$

where α is taken as an upper bound over the whole line for $|f'(u)|$ in the scalar case, or for the absolute value of eigenvalues of the Jacobian for the system case, and $a_2 = -\frac{1}{24}$, $a_4 = \frac{7}{5760}$. If $u^\pm_{i+\frac{1}{2}}$ and $v^\pm_{i+\frac{1}{2}}$ are the fifth order approximations to u and v at $x_{i+\frac{1}{2}}$, respectively, then the formula (2.2) with fluxes (2.5)–(2.8) are the fifth order approximation to equation (2.1).

Remark 1 To the low resolution numerical flux $\hat{f}^L_{i+\frac{1}{2}}$ and $\hat{h}^L_{i+\frac{1}{2}}$ in (2.4), we can use any monotone flux, this is the one of key benefits of this alternative flux formulation. Since LF (Lax–Friedrichs) flux is one of the simplest and most widely used numerical flux, we still use it here. Meanwhile, we also demonstrate some other results such as LLF flux and HLLC flux [21] to some benchmark examples, to illustrate the alternative performance of our schemes.

2.1 Reconstruction of $u^\pm_{i+\frac{1}{2}}$ and $v^\pm_{i+\frac{1}{2}}$ by HWENO Methods

Here we will discuss the reconstruction of polynomial. Interpolation polynomials are constructed by HWENO methodology to approximate $u^\pm_{i+\frac{1}{2}}$ and $v^\pm_{i+\frac{1}{2}}$ in (2.4). As we know, given the point values of $u_i(x)$ and $v_i(x)$, there are many ways to obtain a interpolation polynomial.

Here, we describe one of the methods to obtain a Hermite WENO reconstruction, that is to say Hermite type reconstruction which interpolates to approximate the functions u or v at the cell boundaries. Without loss of generality, we show the procedure of reconstruction to get a fifth-order HWENO scheme. Procedures to construct HWENO schemes of more higher orders of accuracy are similar. The construction of $u^{\pm}_{i+\frac{1}{2}}$ and $v^{\pm}_{i+\frac{1}{2}}$ by HWENO interpolation consist the following steps.

Step 1.1. Given the nodal value u_i and v_i, construct Hermite quadratic polynomials $p_j(x)$ $(j = 0, 1, 2)$ over small stencils $s_0 = \{x_{i-1}, x_i\}, s_1 = \{x_i, x_{i+1}\}, s_2 = \{x_{i-1}, x_i, x_{i+1}\}$ and a fourth-degree polynomial $q(x)$ over the bigger stencil $\mathcal{T} = s_0 \cup s_1 \cup s_2$. These polynomials $p_0(x)$, $p_1(x)$, $p_2(x)$ and $q(x)$ should satisfy

$$\begin{aligned} &p_0(x_k) = u_k, \quad k = i-1,\ i, \quad p_0'(x_{i-1}) = v_{i-1},\\ &p_1(x_k) = u_k, \quad k = i,\ i+1, \quad p_1'(x_{i+1}) = v_{i+1},\\ &p_2(x_k) = u_k, \quad k = i-1,\ i,\ i+1; \end{aligned}$$

and

$$q(x_k) = u_k, \quad k = i-1,\ i,\ i+1, \qquad q'(x_k) = v_k, \quad k = i-1, i+1.$$

Since we only need the values of these polynomials at the cell boundaries, i.e. $x = x_{i+\frac{1}{2}}$, by performing some algebraic manipulations we derive the following expressions:

$$\begin{aligned} p_0\left(x_{i+\frac{1}{2}}\right) &= -\frac{5}{4}u_{i-1} + \frac{9}{4}u_i - \frac{3}{4}\Delta x v_{i-1},\\ p_1\left(x_{i+\frac{1}{2}}\right) &= \frac{1}{4}u_i + \frac{3}{4}u_{i+1} - \frac{1}{4}\Delta x v_{i+1},\\ p_2\left(x_{i+\frac{1}{2}}\right) &= -\frac{1}{8}u_{i-1} + \frac{3}{4}u_i + \frac{3}{8}u_{i+1},\\ q\left(x_{i+\frac{1}{2}}\right) &= -\frac{1}{8}u_{i-1} + \frac{9}{16}u_i + \frac{9}{16}u_{i+1} - \frac{3}{64}\Delta x(v_{i-1} + 3v_{i+1}). \end{aligned} \tag{2.9}$$

Step 1.2. A crucial component for HWENO procedures is to write the $q(x)$ as a linear convex combination of polynomial $p_0(x)$, $p_1(x)$, $p_2(x)$. Simple algebra gives the combination coefficients $\gamma_k (k = 0, 1, 2)$ (usually referred to as the linear weights) such that

$$q\left(x_{i+\frac{1}{2}}\right) = \sum_{k=0}^{2} \gamma_k p_k\left(x_{i+\frac{1}{2}}\right)$$

and $\sum_{k=0}^{2} \gamma_k = 1$. Here the coefficients are $\gamma_0 = \frac{1}{16}, \gamma_1 = \frac{9}{16}, \gamma_2 = \frac{3}{8}$.

Step 1.3. In order to measure the smoothness of the function $p_j(x)$ in the corresponding stencil, we need to calculate the smoothness indicator β_j for each stencil s_j. This is another key component introducing the smoothness indicator which change the linear weights obtained in the Step 1.2. to nonlinear weights, to ensure both accuracy in smooth cases and non-oscillatory performance when at least one of the small stencils contains a discontinuity of the function $u(x)$, $v(x)$. We choose the smoothness indicator in [8]

$$\beta_j = \sum_{k=1}^{2} \int_{I_i} \Delta x^{2k-1} \left(\frac{\partial^k}{\partial x^k} p_j(x)\right)^2 dx. \tag{2.10}$$

In the literature, the smoothness indicator β_j is a quadratic function of the values of the u and v in each stencil s_j. In this article, the smoothness indicator expressions explicitly in details are given

$$\begin{aligned}
\beta_0 &= (-2u_{i-1} + 2u_i - \Delta x v_{i-1})^2 + \frac{13}{3}(-u_{i-1} + u_i - \Delta x v_{i-1})^2, \\
\beta_1 &= (-2u_i + 2u_{i+1} - \Delta x v_{i+1})^2 + \frac{13}{3}(u_i - u_{i+1} + \Delta x v_{i+1})^2, \\
\beta_2 &= \frac{1}{4}(-u_{i-1} + u_{i+1})^2 + \frac{13}{12}(u_{i-1} - 2u_i + u_{i+1})^2.
\end{aligned} \tag{2.11}$$

Step 1.4. Evaluating the nonlinear weights such that the final approximation to $u^-_{i+\frac{1}{2}}$ has the essentially non-oscillatory property. Here the nonlinear weight is defined by

$$w_j = \frac{\bar{w}_j}{\sum_k \bar{w}_k}, \quad \bar{w}_k = \frac{\gamma_k}{(\beta_k + \varepsilon)^2}, \quad k = 0, 1, 2,$$

where γ_k are the weights determined by the second step above, and ε is a small positive real number which is introduced to avoid the denominator becoming zero, ε is taken as 10^{-6} in all our numerical results.

Step 1.5. Finally, the HWENO reconstruction approximation $u^-_{i+\frac{1}{2}}$ is obtained by

$$u^-_{i+\frac{1}{2}} \approx \sum_{k=0}^{2} w_k p_k \left(x_{i+\frac{1}{2}}\right).$$

The reconstruction procedure of $u^+_{i+\frac{1}{2}}$ is mirror symmetric with respect to $x_{i+\frac{1}{2}}$ of that for $u^-_{i+\frac{1}{2}}$ described above.

The reconstruction procedure of the derivative values $v^{\pm}_{i+1/2}$.

Step 2.1. Given the nodal values of u_i and v_i, we construct Hermite type cubic reconstruction polynomials $p_j(x)$, $(j = 1, 2, 3)$ and fifth-degree polynomials $q(x)$ in the small stencils $s_0 = \{x_{i-1}, x_i\}$, $s_1 = \{x_i, x_{i+1}\}$, $s_2 = \{x_{i-1}, x_i, x_{i+1}\}$, and the bigger one $\mathcal{T} = s_0 \cup s_1 \cup s_2$, respectively, such that:

$$\begin{aligned}
&p_0(x_k) = u_k, \quad p_0'(x_k) = v_k, \quad k = i-1,\ i, \\
&p_1(x_k) = u_k, \quad p_1'(x_k) = v_k, \quad k = i,\ i+1, \\
&p_2(x_k) = u_k, \quad k = i-1,\ i,\ i+1, \quad p_2'(x_i) = v_i;
\end{aligned}$$

and

$$q(x_k) = u_k, \qquad q'(x_k) = v_k, \quad k = i-1,\ i,\ i+1.$$

Since we only need the values of these polynomials at the cell boundaries, i.e. $x = x_{i+\frac{1}{2}}$, by performing some algebraic manipulations we derive the following expression:

$$\begin{aligned}
p_0'\left(x_{i+\frac{1}{2}}\right) &= \frac{9}{2\Delta x}(u_{i-1} - u_i) + \frac{7}{4}v_{i-1} + \frac{15}{4}v_i, \\
p_1'\left(x_{i+\frac{1}{2}}\right) &= \frac{3}{2\Delta x}(-u_i + u_{i+1}) - \frac{1}{4}v_i - \frac{1}{4}v_{i+1}, \\
p_2'\left(x_{i+\frac{1}{2}}\right) &= \frac{1}{8\Delta x}(u_{i-1} - u_i + 7u_{i+1}) + \frac{1}{4}v_i, \\
q'\left(x_{i+\frac{1}{2}}\right) &= \frac{1}{\Delta x}\left(\frac{3}{64}u_{i-1} - \frac{3}{2}u_i + \frac{93}{64}u_{i+1}\right) + \frac{1}{64}(v_{i-1} - 12v_i - 15v_{i+1}).
\end{aligned} \tag{2.12}$$

Step 2.2. Again simple algebra gives the linear weights $\gamma_k'(k=0,1,2)$ such that

$$q'\left(x_{i+\frac{1}{2}}\right)=\sum_{k=0}^{2}\gamma_k' p_k'\left(x_{i+\frac{1}{2}}\right)$$

and $\sum_{k=0}^{2}\gamma_k'=1$. Here the coefficients are $\gamma_0'=\frac{1}{112}$, $\gamma_1'=\frac{15}{16}$, $\gamma_2'=\frac{3}{56}$.

Step 2.3. To the reconstruction of derivatives, we define the smoothness indicator as follows:

$$\beta_j=\sum_{k=2}^{3}\int_{I_i}\Delta x^{2k-1}\left(\frac{\partial^k}{\partial x^k}p_j(x)\right)^2 dx \tag{2.13}$$

Note that the summation begins from the second derivative rather than from the first, see [12] for more details. Substitution of $p_j(x)(j=0,1,2)$ defined by (2.12) into (2.13) gives

$$\begin{aligned}
\beta_0&=\frac{13}{12}(12(u_{i-1}-u_i)+6\Delta x(v_{i-1}+v_i))^2+(6(u_{i-1}-u_i)+\Delta x(2v_{i-1}+4v_i))^2,\\
\beta_1&=\frac{13}{12}(12(u_i-u_{i+1})+6\Delta x(v_i+v_{i+1}))^2+(-6(u_i-u_{i-1})-\Delta x(4v_i+2v_{i+1}))^2,\\
\beta_2&=\frac{13}{12}(-3u_{i-1}+3u_{i+1}-6\Delta x v_i)^2+(u_{i-1}-2u_i+u_{i+1})^2.
\end{aligned}$$

Step 2.4. Compute the nonlinear weights by

$$w_j=\frac{\bar{w}_j}{\sum_k\bar{w}_k},\ \bar{w}_k=\frac{\gamma_k'}{(\beta_k+\varepsilon)^2},\quad k=0,1,2$$

where γ_k' is given by 2. The ε is again taken as 10^{-6} to avoid the division by zero in the denominator.

Step 2.5. Finally, the reconstruction derivatives $v^-_{i+\frac{1}{2}}$ is defined as:

$$v^-_{i+\frac{1}{2}}\approx\sum_{k=0}^{2}w_k p_k'(x_{i+1/2}).$$

Again the reconstruction procedure of $v^+_{i+\frac{1}{2}}$ is mirror symmetric with respect to $x_{i+\frac{1}{2}}$ of that for $v^-_{i+\frac{1}{2}}$ described above.

Remark 2 For system cases, such as the Euler equations of gas dynamics, in order to avoid oscillation, both the reconstructions of $u^-_{i+1/2}$, $v^-_{i+1/2}$ from u_i, v_i are performed in the local characteristic directions, for more details of such local characteristic decompositions see [17].

2.2 Reconstruction of $\hat{f}^H_{i+\frac{1}{2}}$ and $\hat{h}^H_{i+\frac{1}{2}}$

For stability considering, we use following procedure to reconstruct $\hat{f}^H_{i+\frac{1}{2}}$ and $\hat{h}^H_{i+\frac{1}{2}}$. First we split fluxes f and h into two parts, respectively, such that:

$$f=f^+ + f^-,\ h=h^+ + h^-$$

with

$$f^+ = \frac{1}{2}(f(u) + \alpha u),\ \ f^- = \frac{1}{2}(f(u) - \alpha u),$$
$$h^+ = \frac{1}{2}(h(u,v) + \alpha v),\ \ h^- = \frac{1}{2}(h(u,v) - \alpha v),$$

where $\alpha = \max |f'(u)|$, and we can see that

$$\frac{d}{du}f^+ \geq 0,\ \ \frac{d}{du}f^- \leq 0,\ \ \frac{\partial}{\partial v}h^+ \geq 0,\ \ \frac{\partial}{\partial v}h^- \leq 0.$$

Then we use following finite differences to approximate $\Delta x^2(\frac{\partial^2 f}{\partial x^2})_{i+\frac{1}{2}}$, $\Delta x^4(\frac{\partial^4 f}{\partial x^4})_{i+\frac{1}{2}}$, respectively.

$$\hat{f1}^-_{i+1/2} + \hat{f1}^+_{i+1/2} \approx \Delta x^2 \left(\frac{\partial^2 f}{\partial x^2}\right)_{i+\frac{1}{2}}$$

where

$$\hat{f1}^-_{i+1/2} = \frac{5}{4}f^+_{i-1} - f^+_i - \frac{1}{4}f^+_{i+1} + \frac{1}{2}h^+_{i-1} + h^+_{i+1},$$
$$\hat{f1}^+_{i+1/2} = \frac{5}{4}f^-_{i+2} - f^-_{i+1} - \frac{1}{4}f^-_i - \frac{1}{2}h^-_{i+2} - h^-_i.$$
$$\hat{f2}^-_{i+1/2} + \hat{f2}^+_{i+1/2} \approx \Delta x^4 \left(\frac{\partial^4 f}{\partial x^4}\right)_{i+\frac{1}{2}}$$

where

$$\hat{f2}^-_{i+1/2} = -12\left(f^+_{i-1} - 2f^+_i + f^+_{i+1}\right) - 6\left(h^+_{i-1} - h^+_{i+1}\right),$$
$$\hat{f2}^+_{i+1/2} = -12\left(f^-_{i-1} - 2f^-_i + f^-_{i+1}\right) - 6\left(h^-_{i-1} - h^-_{i+1}\right).$$

Finally, we have:

$$\hat{f}^H_{i+\frac{1}{2}} = a_2(\hat{f1}^-_{i+1/2} + \hat{f1}^+_{i+1/2}) + a_4(\hat{f2}^-_{i+1/2} + \hat{f2}^+_{i+1/2}). \tag{2.14}$$

We can also have the following approximation:

$$\hat{h1}^-_{i+1/2} + \hat{h1}^+_{i+1/2} \approx \Delta x^2 \left(\frac{\partial^2 h}{\partial x^2}\right)_{i+\frac{1}{2}},\quad \hat{h2}^-_{i+1/2} + \hat{h2}^+_{i+1/2} \approx \Delta x^4 \left(\frac{\partial^4 h}{\partial x^4}\right)_{i+\frac{1}{2}},$$

where

$$\hat{h1}^-_{i+1/2} = \frac{1}{4}\left(39f^+_{i-1} - 48f^+_i + 9f^+_{i+1} + 21h^+_{i-1} + 12h^+_i - 3h^+_{i+1}\right),$$
$$\hat{h}^+_{i+1/2} = \frac{1}{4}\left(-9f^-_{i-1} + 48f^-_i - 39f^-_{i+1} - 3h^-_{i-1} + 12h^-_i + 21h^-_{i+1}\right).$$
$$\hat{h2}^-_{i+1/2} = 30\left(3\left(f^+_{i-1} - f^+_{i+1}\right) + h^+_{i-1} + 4h^+_i + h^+_{i+1}\right),$$
$$\hat{h2}^+_{i+1/2} = 30\left(3\left(f^-_{i-1} - f^-_{i+1}\right) + h^-_{i-1} + 4h^-_i + h^-_{i+1}\right).$$

and

$$\hat{h}^H_{i+\frac{1}{2}} = a_2\left(\hat{h1}^-_{i+1/2} + \hat{h1}^+_{i+1/2}\right) + a_4\left(\hat{h2}^-_{i+1/2} + \hat{h2}^+_{i+1/2}\right). \tag{2.15}$$

Remark 3 For systems of conservation laws, the procedure of reconstruction of $\hat{f}^H_{i+\frac{1}{2}}$ and $\hat{h}^H_{i+\frac{1}{2}}$ are performed in component by component.

Remark 4 We still use the methodology of flux splitting for these high order derivative terms, the main reason is to consider the stability and the upwind performance of the scheme. By testing, we found that the central difference method is not suitable for some strong shock problems, such as the Double Mach Reflection problem.

Remark 5 Positivity-preserving flux limiter is key point for high-order numerical methods, which is used to maintain the density ρ and the pressure p to be positive. There are serval positivity-preserving methods in the literature, such as [7,23,24]. In this paper we take the technique by Hu, Adams and Shu, for details refer to [7].

2.3 Temporal Discretizations

The semi-discrete scheme (2.2), can be written as an ordinary differential equation (ODE) system

$$U_t = L(U), \tag{2.16}$$

is then discretized in time by a total variation diminishing (TVD) Runge–Kutta method [19,20], for example the third order version given by

$$\begin{aligned} U^{(1)} &= U^n + \Delta t L(U^n) \\ U^{(2)} &= \frac{3}{4}U^n + \frac{1}{4}U^{(1)} + \frac{1}{4}\Delta t L(U^{(1)}) \\ U^{n+1} &= \frac{1}{3}U^n + \frac{2}{3}U^{(2)} + \frac{2}{3}\Delta t L(U^{(2)}). \end{aligned} \tag{2.17}$$

3 The Fourth Order HWENO Scheme for Two Dimensional conservation laws

In this section we extend the method in section 2 to solve nonlinear two dimensional hyperbolic conservation laws. Firstly we consider two dimensional scalar conservation law:

$$\begin{cases} u_t + f(u)_x + g(u)_y = 0, \ \ (x, y) \in R^2, \ t \in (0, \infty) \\ u(x, y, 0) = u_0(x, y), \ \ (x, y) \in R^2, \end{cases} \tag{3.1}$$

where $u(x, y, t)$ is a conserved quantity, $f(u(x, y, t))$ and $g(u(x, y, t))$ describe its flux in x direction and y direction. Let $v = u_x$, $w = u_y$, taking the derivative x and y of (3.1) separately, then we obtain a complete set of equations form that we need to solve as below

$$\begin{cases} u_t + f(u)_x + g(u)_y = 0, \\ v_t + h(u, v)_x + r(u, v)_y = 0, \\ w_t + q(u, w)_x + s(u, w)_y = 0, \end{cases} \tag{3.2}$$

where

$$\begin{aligned} h(u, v) &= f'(u)v, \ \ r(u, v) = g'(u)v, \\ q(u, w) &= f'(u)w, \ \ s(u, w) = g'(u)w. \end{aligned}$$

For simplicity, we assume that the mesh is uniform with the cell size $x_{i+1/2}-x_{i-1/2}=\Delta x$, $y_{j+1/2}-y_{j-1/2}=\Delta y$, and cell centers $(x_i, y_j)=(\frac{1}{2}(x_{i+1/2}+x_{i-1/2}), \frac{1}{2}(y_{j+1/2}-y_{j-1/2}))$. We also denote the cells by $I_{ij}=[x_{i-\frac{1}{2}}, x_{i+\frac{1}{2}}]\times[y_{j-\frac{1}{2}}, y_{j+\frac{1}{2}}]$.

Again the conservative scheme for Eq. (3.2) can be written as a semi-discretization form

$$\begin{cases} \frac{du_{i,j}(t)}{dt}+\frac{1}{\Delta x}\left(\hat{f}_{i+\frac{1}{2},j}-\hat{f}_{i-\frac{1}{2},j}\right)+\frac{1}{\Delta y}\left(\hat{g}_{i,j+\frac{1}{2}}-\hat{g}_{i,j-\frac{1}{2}}\right)=0, \\ \frac{dv_{i,j}(t)}{dt}+\frac{1}{\Delta x}\left(\hat{h}_{i+\frac{1}{2},j}-\hat{h}_{i-\frac{1}{2},j}\right)+\frac{1}{\Delta y}\left(\hat{r}_{i,j+\frac{1}{2}}-\hat{r}_{i,j-\frac{1}{2}}\right)=0, \\ \frac{dw_{i,j}(t)}{dt}+\frac{1}{\Delta x}\left(\hat{q}_{i+\frac{1}{2},j}-\hat{q}_{i-\frac{1}{2},j}\right)+\frac{1}{\Delta y}\left(\hat{s}_{i,j+\frac{1}{2}}-\hat{s}_{i,j-\frac{1}{2}}\right)=0. \end{cases} \tag{3.3}$$

We can straightforward extend the one dimension procedure to the numerical fluxes $\hat{f}_{i\pm\frac{1}{2},j}$, $\hat{h}_{i\pm\frac{1}{2},j}$, $\hat{g}_{i,j\pm\frac{1}{2}}$ and $\hat{s}_{i,j\pm\frac{1}{2}}$, in a dimension-by-dimension fashion, and we would not describe it again here.

For the reconstruction of fluxes for the mixed derivative terms in the Eq.(3.2), i.e. $\hat{q}_{i+\frac{1}{2},j}$, we will adopt the following procedure:

$$\begin{aligned} \hat{q}_{i+\frac{1}{2},j}=&\frac{1}{2}\left(q\left(u^{+}_{i+\frac{1}{2},j}, w^{+}_{i+\frac{1}{2},j}\right)+q\left(u^{-}_{i+\frac{1}{2},j}, w^{-}_{i+\frac{1}{2},j}\right)\right)-\frac{\alpha}{2}\left(w^{+}_{i+\frac{1}{2},j}-w^{-}_{i+\frac{1}{2},j}\right)\Big) \\ &-\frac{1}{24}\Delta x^2\left(\frac{\partial^2 q}{\partial x^2}\right)_{i+\frac{1}{2},j}, \end{aligned} \tag{3.4}$$

where $\alpha=\max_u|f'(u)|$. In order to keep the compactness of the scheme, we would like to reconstruct $w^{\pm}_{i+1/2,j}$ by third order WENO reconstruction, this leads to the scheme is the fourth order. We choose two small stencils $s_1=\{x_{i-1,j}, x_{i,j}\}$ and $s_2=\{x_{i,j}, x_{i+1,j}\}$ and big stencil $\mathcal{T}=\{s_1, s_2\}$, then we find interpolate polynomials $p_1(x)$, $p_2(x)$ and $Q(x)$ such that:

$$p_1(x_k)=w_{k,j}\ (k=i-1,i),\ \ p_2(x_k)=w_{k,j}\ (k=i,i+1),$$
$$Q(x_k)=w_{k,j}\ (k=i-1,i,i+1)$$

A simple algebra leads to explicit formula for this two polynomials at the cell boundaries

$$\begin{aligned} p_1\left(x_{i+\frac{1}{2}}\right)&=-\frac{1}{2}w_{i-1,j}+\frac{3}{2}w_{i,j}, \\ p_2\left(x_{i+\frac{1}{2}}\right)&=\frac{1}{2}w_{i,j}+\frac{1}{2}w_{i+1,j}, \\ Q\left(x_{i+\frac{1}{2}}\right)&=-\frac{1}{8}w_{i-1,j}+\frac{3}{4}w_{i,j}+\frac{3}{8}w_{i+1,j}. \end{aligned}$$

The approximation $Q(x_{i+\frac{1}{2}})$ can be written as a linear convex combination of the two second order approximations $p_1(x_{i+\frac{1}{2}})$ and $p_2(x_{i+\frac{1}{2}})$. Denoting the linear weights by γ_1, γ_2 such that

$$Q\left(x_{i+\frac{1}{2}}\right)=\gamma_1 p_1\left(x_{i+\frac{1}{2}}\right)+\gamma_2 p_2\left(x_{i+\frac{1}{2}}\right),$$

where the constants γ_1, γ_2 satisfying $\gamma_1+\gamma_2=1$. And here the linear weights are given as $\gamma_1=\frac{1}{4}, \gamma_2=\frac{3}{4}$.

Then the WENO procedure is to change the linear weights to nonlinear weights. This is achieved through a choice of the so-called smoothness indicator β_j. In this paper, we use the

same formula with (2.10) obtaining the smoothness indicator expressions:

$$\beta_1 = (-w_{i-1,j} + w_{i,j})^2;$$
$$\beta_2 = (-w_{i,j} + w_{i+1,j})^2.$$

The nonlinear weights ω_j are defined by

$$\omega_j = \frac{\bar{\omega}_j}{\bar{\omega}_1 + \bar{\omega}_2}, \quad \bar{\omega}_j = \frac{\gamma_j}{(\varepsilon + \beta_j)^2}, \ j = 1, 2;$$

where ε is a small positive number to avoid the denominator to become zero.

Finally, the approximation of $w^-_{i+\frac{1}{2},j}$ is achieved as

$$w^-_{i+\frac{1}{2},j} = \omega_1 p_1\left(x_{i+\frac{1}{2}}\right) + \omega_2 p_2\left(x_{i+\frac{1}{2}}\right). \tag{3.5}$$

The procedure of reconstruction of $w^+_{i+\frac{1}{2},j}$ is mirror symmetric with respect to $x_{i+\frac{1}{2},j}$ of that for $w^-_{i+\frac{1}{2},j}$ described above.

For the reconstruction of the second term $\Delta x^2(\frac{\partial^2 q}{\partial x^2})_{i+\frac{1}{2},j}$ in (3.4), we will adopt the following procedure. For stability, we first split the q into two parts, $q = q^+ + q^-$, with $\frac{\partial}{\partial w}q^+ \geq 0$, $\frac{\partial}{\partial w}q^- \leq 0$, for example, we use:

$$q^+_{ij} = \frac{1}{2}(q(u_{ij}, w_{ij}) + \alpha w_{ij}), \ q^-_{ij} = \frac{1}{2}(q(u_{ij}, w_{ij}) - \alpha w_{ij}),$$

and have the following approximation:

$$\Delta x^2\left(\frac{\partial^2 q}{\partial x^2}\right)_{i+\frac{1}{2},j} \approx q^+_{i-1,j} - 2q^+_{i,j} + q^+_{i+1,j} + q^-_{i,j} - 2q^-_{i+1,j} + q^-_{i+2,j}.$$

Again, for system cases, the reconstruction procedure of $w^{\pm}_{i+1/2,j}$ are performed in the local characteristic directions, and $\Delta x^2(\frac{\partial^2 q}{\partial x^2})_{i+\frac{1}{2},j}$ are performed in component by component.

The reconstruction procedure of $\hat{r}_{i,j+\frac{1}{2}}$ is similar to that for $\hat{q}_{i+\frac{1}{2},j}$, we perform it on y direction.

4 Numerical Results

In this section, we will devote to implement extensive numerical experiments for hyperbolic conservation laws to illustrate the performance of our methods. In all the numerical examples, we adopt the third order Runge–Kutta method for the time discretization and CFL number is taken to be 0.2 for one and two dimensional cases, except for the accuracy tests where a suitably reduced time step is used to guarantee that spatial error dominates.

4.1 Accuracy Tests for One Dimensional Case

Example 4.1 We consider the nonlinear Burgers' equation

$$\begin{cases} u_t + (u^2/2)_x = 0, \\ u(x, 0) = 0.5 + \sin(\pi x), \quad 0 \leq x \leq 2. \end{cases} \tag{4.1}$$

Table 1 One-dimensional Burgers' equation, the comparison of error and order for HWENO method and WENO method

N	HWENO5				WENO5			
	L_1 error	Order	L_∞ error	Order	L_1 error	Order	L_∞ error	Order
10	2.85E−03		7.81E−03		1.90E−02		7.42E−02	
20	1.98E−04	3.84	9.03E−04	3.11	2.07E−03	3.20	1.22E−02	2.61
40	1.24E−05	4.01	9.72E−05	3.22	1.32E−04	3.97	1.04E−03	3.55
80	5.31E−07	4.54	4.87E−06	4.32	4.61E−06	4.84	4.73E−05	4.46
160	2.29E−08	4.54	4.00E−07	3.61	1.79E−07	4.69	1.50E−06	4.98
320	7.00E−10	5.03	1.77E−08	4.50	6.90E−09	4.70	1.37E−07	3.45
640	2.06E−11	5.08	4.70E−10	5.23	2.02E−10	5.09	7.63E−09	4.17

Table 2 One-dimensional Euler equation, the comparison of error and order for HWENO method and WENO method

N	HWENO5				WENO5			
	L_1 error	Order	L_∞ error	Order	L_1 error	Order	L_∞ error	Order
10	2.75E−03		3.91E−03		5.73E−03		8.11E−03	
20	1.01E−04	4.77	1.79E−04	4.45	2.76E−04	4.37	4.40E−04	4.20
40	2.98E−06	5.08	5.53E−06	5.02	8.53E−06	5.02	1.58E−05	4.80
80	9.16E−08	5.02	1.72E−07	5.00	2.66E−07	5.00	4.95E−07	4.99
160	2.82E−09	5.02	5.06E−09	5.09	8.23E−09	5.01	1.47E−08	5.08
320	8.48E−11	5.06	1.43E−10	5.14	2.48E−10	5.05	4.16E−10	5.14
640	2.31E−12	5.20	3.78E−12	5.25	6.85E−12	5.18	2.13E−11	4.28

with periodic boundary conditions. We compute the solution up to $t = 0.5/\pi$, when the solution is still smooth. The errors and numerical orders of HWENO5 comparing to WENO5 are shown in Table 1. Numerical results show that the designed fifth order accuracy is achieved for the HWENO5 spatial discretization and the errors by HWENO5 are smaller than those by the classical finite difference WENO5 with the same grid points.

Example 4.2 Euler equations. We solve the following nonlinear system of Euler equations $u_t + f(u)_x = 0$, with

$$u = (\rho, \rho v, E)^T, \ f(u) = (\rho v, \rho v^2 + p, v(E + p))^T,$$

where ρ is the density, v is the velocity , E is the total energy, and p is the pressure, which is related to the total energy by $E = p/(\gamma - 1) + 1/2\rho v^2$ with $\gamma = 1.4$. The initial condition is set to be $\rho(x, 0) = 1 + 0.2\sin(\pi x)$, $v(x, 0) = 1$, $p(x, 0) = 1$. The domain of interest in the $x - t$ plane are points (x, t) we choose here $-1 < x < 1$ and $t > 0$. We compute the solution up to $t = 2$. The errors and numerical orders of accuracy of the density ρ by the HWENO scheme comparison with those by WENO5 scheme are shown in Table 2. We can also see that the designed fifth order accuracy is achieved for the HWENO5 and the errors by HWENO5 are smaller than those by the classical finite difference WENO5 with the same grid points. In addition, we list the errors and numerical order which are computed

Table 3 One-dimensional Euler equation

N	L_1 errors	Order	L_∞ errors	Order
LF				
10	2.75E−03		3.91E−03	
20	1.01E−04	4.77	1.79E−04	4.45
40	2.98E−06	5.08	5.53E−06	5.02
80	9.16E−08	5.02	1.72E−07	5.00
160	2.82E−09	5.02	5.06E−09	5.09
320	8.48E−11	5.06	1.43E−10	5.14
LLF				
10	2.73E−03		3.89E−03	
20	1.00E−04	4.77	1.78E−04	4.45
40	2.95E−06	5.08	5.48E−06	5.02
80	9.08E−08	5.02	1.71E−07	5.00
160	2.80E−09	5.02	5.01E−09	5.09
320	8.41E−11	5.06	1.43E−10	5.13
HLLC				
10	2.75E−03		3.88E−03	
20	1.01E−04	4.77	1.78E−04	4.44
40	2.98E−06	5.08	5.52E−06	5.02
80	9.18E−08	5.02	1.73E−07	5.00
160	2.83E−09	5.02	5.06E−09	5.09
320	8.50E−11	5.06	1.44E−10	5.13

L_1 and L_∞ errors and orders of the three kind of fluxes

by HWENO with LF flux, LLF(local LF) flux and HLLC flux in Table 3. We can see that the numerical results are similar for HWENO with three different numerical fluxes.

4.2 Tests Cases with Shocks for One Dimensional Case

Example 4.3 Burgers' equation.

We solve the same nonlinear Burgers' equation $u_t + (u^2/2)_x = 0$ as Example 4.1, with the initial condition $u(x, 0) = 0.5 + \sin(\pi x)$, $0 \le x \le 2$. We plot the results at $t = 1.5/\pi$ when a shock has already appeared in the solution. In Fig. 1, the computational result is displayed, we can see that the shock is captured very well.

Example 4.4 Non-convex problem.

We solve the nonlinear non-convex scalar Buckley–Leverett problem

$$u_t + \left(\frac{4u^2}{4u^2 + (1-u)^2}\right)_x = 0,$$

with the initial data $u = 1$ in $-\frac{1}{2} \le x \le 0$ and $u = 0$ elsewhere to test convergence to the physically correct entropy solutions. The solution is computed up to $t = 0.4$. The exact solution is a shock-rarefaction-contact discontinuity mixture. In Fig. 2, the solutions are shown, the solid line is the exact solution while the plus and square are numerical solutions

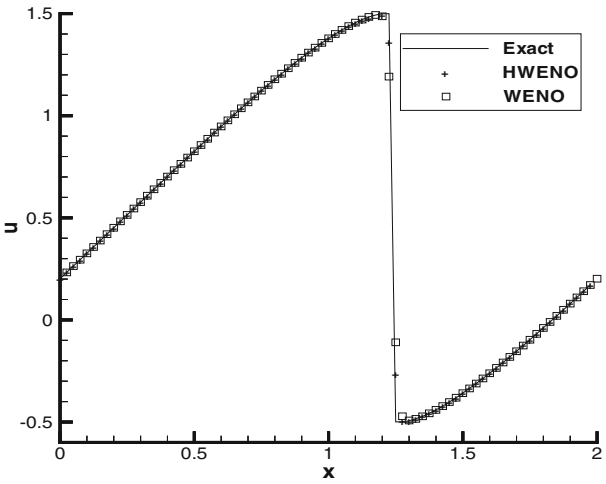

Fig. 1 Burgers equation. $t = 1.5/\pi$, $N = 80$. The comparison of HWENO method and WENO method. *Solid line*: exact solution; "*plus*": HWENO, "*square*": WENO

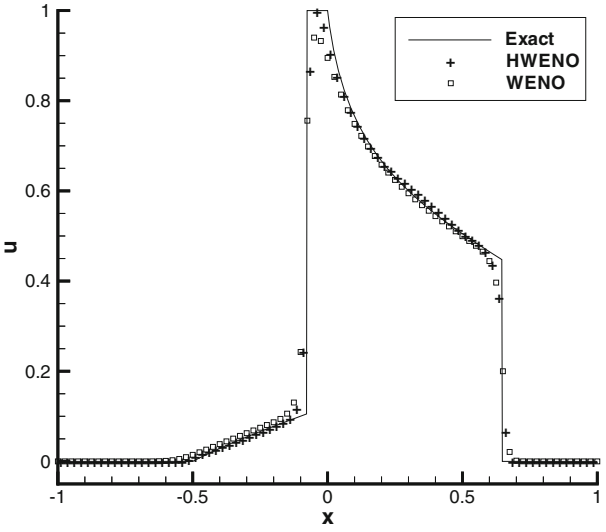

Fig. 2 The Buckley–Leverett problem. $t = 0.4$, $N = 80$. The comparison of HWENO method and WENO method. The *solid line*: exact solution; "*plus*": HWENO, "*square*": WENO

by HWENO5 and finite difference WENO5, respectively. Once more, we can clearly see the same conclusion as above: the HWENO5 scheme approximates the exact solution more precisely.

Example 4.5 Nonlinear Euler equation.

We solve the Euler equations in Example 4.2, with a Riemann initial condition for the Lax Problem $(\rho, m, E) = (0.445, 0.31061, 8.928) \quad for\, x \leq 0$, $(\rho, m, E) = (0.5, 0, 0.571) \quad for\, x > 0$. We choose the domain of computation in $[-5, 5]$. The computed density ρ, pressure p and velocity v are plotted at $t = 1.3$ against the exact solution.

The numerical results with $N = 200$ uniform points and a comparison with the results using WENO5 scheme in the same uniform points are shown in Fig. 3. In Figure 4, we show the numerical results by HWENO with LF flux, LLF flux and HLLC flux, we can see that the result by method with HLLC flux has the slightly better performance than those the others.

Example 4.6 We solve the Euler equations in Example 4.2, with a Riemann initial condition for the Shu-Osher Problem $(\rho, v, p) = (3.857143, 2.629369, 10.333333) \quad for\, x \leq -4$, $(\rho, v, p) = (1 + \epsilon \sin 5x, 0, 1) \quad for\, x \geq -4$, where a Mach 3 shock wave interacts with a density disturbance and generates a flow field that has a combination of smooth structures and discontinuities. This problem is a good model for the kinds of interactions that occur in simulations of compressible turbulence. We choose the domain of computation in $[-5, 5]$, and take $\epsilon = 0.2$. The computed density ρ, pressure p and velocity v are plotted at $t = 1.8$ against the "exact" solution, which are the converged solution computed by the fifth-order finite difference WENO scheme [8] with 2000 grid points. The numerical results with $N = 300$ uniform points and a comparison with the results using WENO5 scheme in the same uniform points are shown in Fig. 5. We can see that the numerical results by the HWENO are better than those by WENO schemes. In Fig. 6, we show the numerical results by HWENO with LF flux, LLF flux and HLLC flux, we can see that the results by method with LLF or HLLC flux has better performance than those by HWENO with LF flux.

Example 4.7 We have run the interacting blast wave problem with the Euler equations in Example 4.2, with a Riemann initial condition $(\rho, v, p) = (1, 0, 1000) \quad for\, 0 \leq x \leq 0.1$, $(\rho, v, p) = (1, 0, 0.01) \quad for\, 0.1 \leq x \leq 0.9$, $(\rho, v, p) = (1, 0, 100) \quad for\, x \geq 0.9$. We take the domain of computation in $[0, 1]$ and a reflecting boundary condition is applied to both ends. The computed density ρ, pressure p and velocity v are plotted at $t = 0.038$ against the "exact" solution, which are the converged solution computed by the fifth-order finite difference WENO scheme [8] with 2000 grid points. The numerical results with $N = 400$ uniform points and a comparison with the results using WENO5 scheme in the same uniform points are shown in Fig. 7. We also see that the result profile from the 400-zone simulation is very close to the converged result profile and the HWENO5 is slightly better than the WENO5. In Fig. 8, we show the numerical results by HWENO with LF flux, LLF flux and HLLC flux, we can see that the results by method with LLF or HLLC flux has better performance than those by HWENO with LF flux.

Example 4.8 We consider shock entropy wave interactions problem[8,17,26]. In order to illustrate the versatility of the methods developed here and their applicability to other hyperbolic systems, we apply them to a wave-like problem. This famous test case is very suitable for high accuracy order schemes (such as WENO/HWENO schemes) and shock capturing schemes. In this example we test the HWENO schemes on a model that involves a moving shock interacting with an entropy wave of small amplitude. We solve the Euler equations in Example 4.2, with a Riemann initial condition

$$(\rho, u, p)^T = \begin{cases} (3.85714, 2.629369, 10.33333)^T, & 0 \leq x \leq 0.5, \\ (e^{-\varepsilon \sin(\kappa\pi)}, 0, 1)^T, & 0.5 \leq x \leq 5, \end{cases} \tag{4.2}$$

where ε and κ are the amplitude and wave number of the entropy wave, respectively. The detailed description of this see [8]. In our tests, we take $\varepsilon = 0.01$ and $\kappa = 13, 26$. In Figs. 9, 10, 11 and 12 we show the results of the HWENO schemes by pluses comparing with the WENO

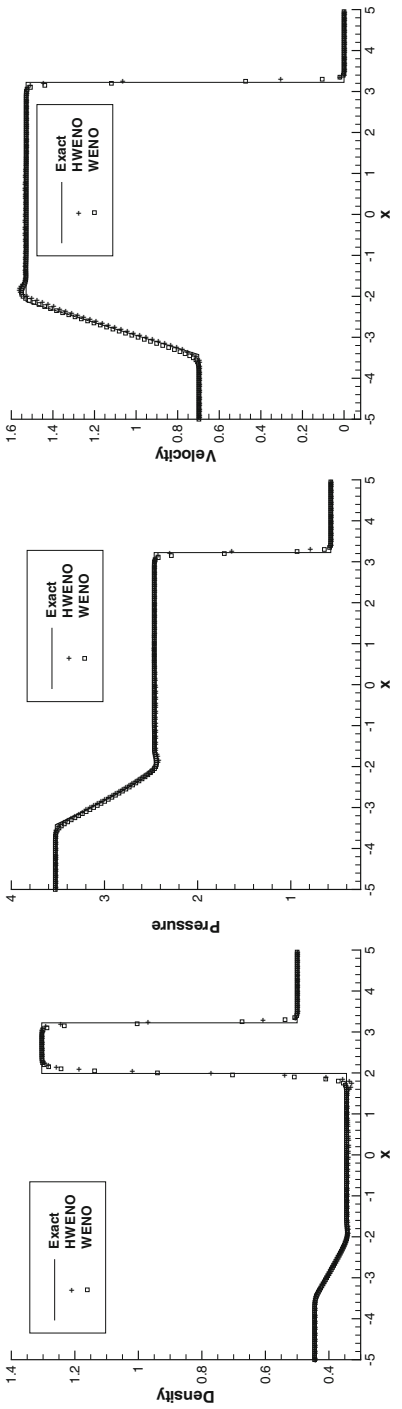

Fig. 3 The Euler equations Lax problem. *Solid line*: exact solution; "*plus*": HWENO, "*square*": WENO

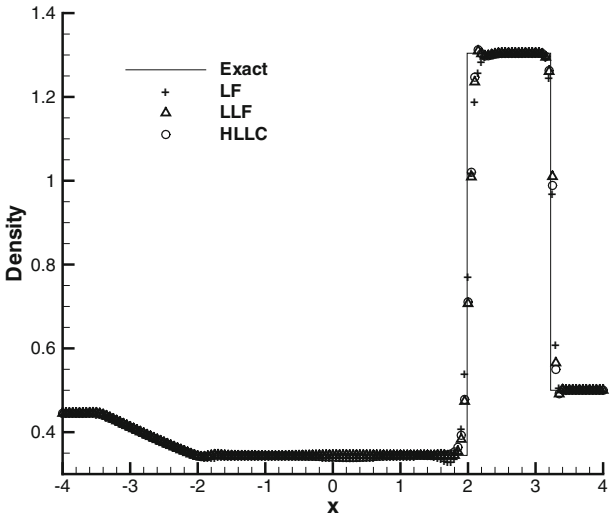

Fig. 4 The Euler equations Lax problem. *Solid line*: exact solution; "*plus*": HWENO with LF flux, "*triangle*": HWENO with LLF flux, "*circle*": HWENO with HLLC flux

schemes by squares. The reference entropy solution is a convergent solution computed by the WENO (fifth-order) schemes with 5000 points for $\kappa = 13, 26$. We observe that the structure of the solution in the calculations has developed very well. To obtain a comparable quality in the solution from a HWENO scheme would have required doing the problem on a grid of different number zones, like 400, 800 etc. This illustrates the considerable advantages of the fifth order HWENO schemes designed here. Thus using the fifth order schemes designed here improves the representation of like-wave problem than the fifth order WENO schemes.

Example 4.9 In this test, we solve the Euler equations with a moving sine wave in density

$$(\rho, u, p)^T = \begin{cases} (1, 1, 1)^T, & -1 \le x \le 0, \\ (1 + 0.2|\sin(\kappa\pi x)|, 1, 1)^T, & 0 \le x \le 1, \\ (1, 1, 1)^T, & 1 \le x \le 2. \end{cases} \tag{4.3}$$

In Fig. 13, we show the results of the HWENO schemes by pluses comparing with the WENO schemes by squares for $\varepsilon = 3$ and 5. The reference entropy solution is a convergent solution computed by the WENO (fifth-order) schemes with 5000 nodes. We observe that the structure of the solution in the calculations has developed very well. The results of HWENO schemes have an advantage over the classic WENO schemes especially in the local smooth extremum and the quantity of the amplitude decreases much less. And we also find that the HWENO scheme can keep even more sharp resolutions and high frequency vibration after a vast time of evolution.

4.3 Tests for Two Dimensional Case

Example 4.10 Burgers' equation.

We solve the non-linear scalar Burgers' equation $u_t + (u^2/2)_x + (u^2/2)_y = 0$, $0 \le x \le 4$, $u(x, y, 0) = u_0(x, y)$, with periodic boundary conditions. Here we consider the

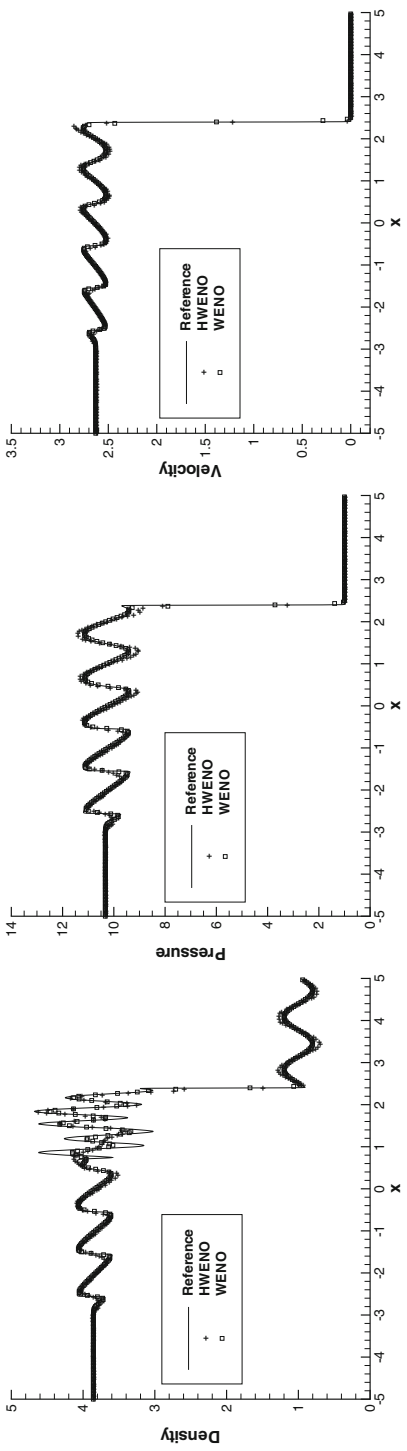

Fig. 5 The Euler equations Shu–Osher problem. *Solid line*: the "exact" reference solution; "*plus*": HWENO, "*square*": WENO

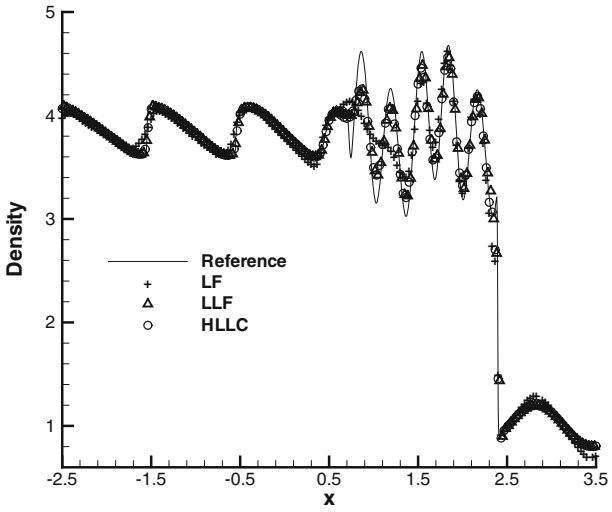

Fig. 6 The Euler equations Shu–osher problem. *Solid line*: the "exact" reference solution; "*plus*": HWENO with LF flux, "*triangle*": HWENO with LLF flux, "*circle*": HWENO with HLLC flux.

hyperbolic conservation laws on test problems with exact solution case. The initial condition is $u_0(x+y) = 0.5 + \sin((x+y)\pi/2)$. We list the L_1 and L_∞ errors for the nodal value at time $t = 0.5/\pi$ in Table 4. We can see clearly that the designed fourth order accuracy is achieved in the two norms for both of schemes.

Example 4.11 Euler equations.

We consider the two-dimensional Euler equations by the present Hermit WENO schemes. The PDEs of two-dimensional Euler equations in the Cartesian coordinate (x, y) are as follows

$$\begin{bmatrix} \rho \\ \rho u \\ \rho v \\ E \end{bmatrix}_t + \begin{bmatrix} \rho u \\ \rho u^2 + p \\ \rho uv \\ u(E+p) \end{bmatrix}_x + \begin{bmatrix} \rho v \\ \rho uv \\ \rho v^2 + p \\ v(E+p) \end{bmatrix}_y = 0, \tag{4.4}$$

where ρ is the density, u and v are the velocity in $x-$ and $y-$direction, respectively, E is the total energy, and p is the pressure, which is related to the total energy by $E = \frac{p}{\gamma - 1} + \frac{1}{2}\rho(u^2+v^2)$ with $\gamma = 1.4$. The initial condition is set to be $\rho(x, y, 0) = 1+0.2\sin(\pi(x+y))$, $u(x, y, 0) = 0.7$, $v(x, y, 0) = 0.3$, $p(x, y, 0) = 1$. We compute the solution up to $t = 2$. The exact solution is $\rho(x, y, t) = 1+0.2\sin(\pi(x+y-(u+v)t))$, $u = 0.7$, $v = 0.3$, $p = 1$. The errors and numerical orders of accuracy of the density ρ for the HWENO schemes are shown in Table 5, which are quite satisfactory.

Example 4.12 Shock vortex interaction.

In this test, we use the HWENO schemes to simulate the model of the interaction between a stationary shock and vortex. The computational domain is chosen to be $[0, 2] \times [0, 1]$. A stationary Mach 1.1 shock is positioned at $x = 0.5$ and normal to the x-axis. A uniform mesh of 251×100 in the computational domain is used. There is a small vortex at the flow left to the shock, its center is $(x_c, y_c) = (0.25, 0.5)$. The initial left

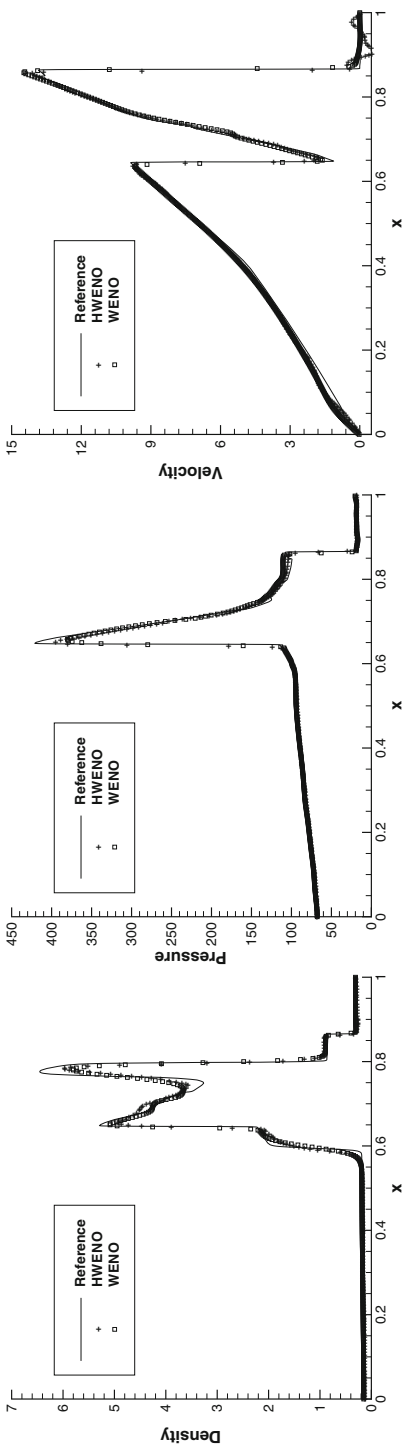

Fig. 7 The Euler equations the blast waves problem. *Solid line*: the "exact" reference solution; "*plus*": HWENO, "*square*": WENO

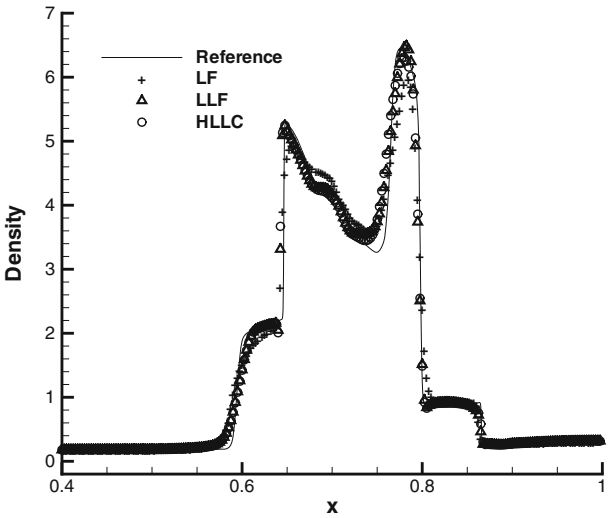

Fig. 8 The Euler equations Blast-wave problem. *Solid line*: the "exact" reference solution; "*plus*": HWENO with LF flux, "*triangle*": HWENO with LLF flux, "*circle*": HWENO with HLLC flux

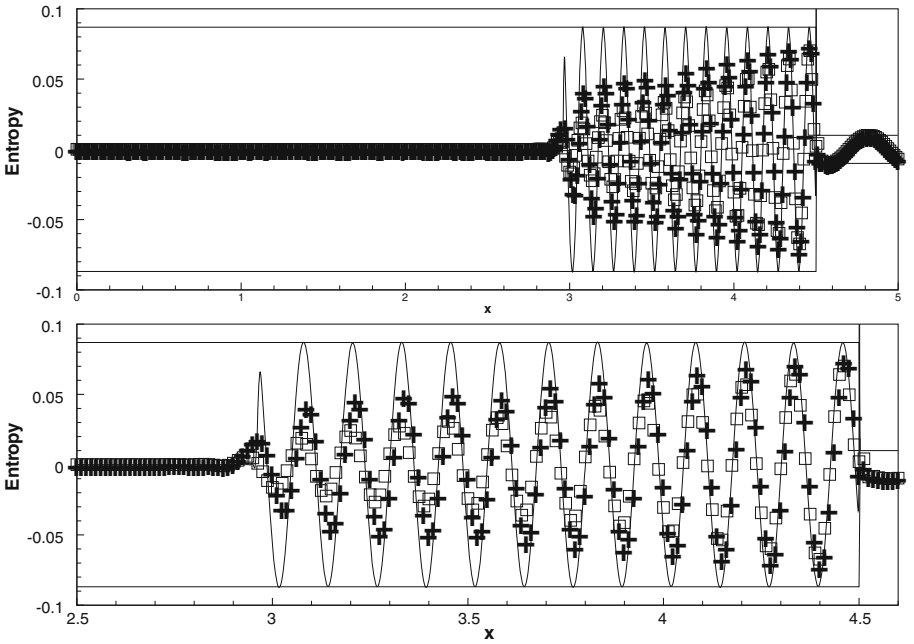

Fig. 9 The shock wave interaction tests. $\kappa = 13$ with 400 points. "*plus*": HWENO, "*square*": WENO. The reference solution is *solid line* and the *zoom* are given in *bottom*

state is $(\rho, u, v, p) = (1, 1.1\sqrt{\gamma}, 0, 1)$. Its right state can be easily make sure by the $Rankine - Hugoniot$ condition. The problem is initialized by the vortex as a perturbation to the velocity (u, v), temperature $(T = p/\rho)$, and entropy $(S = \ln(p/\rho^{\gamma}))$ of the mean flow and we can denote them by the following values:

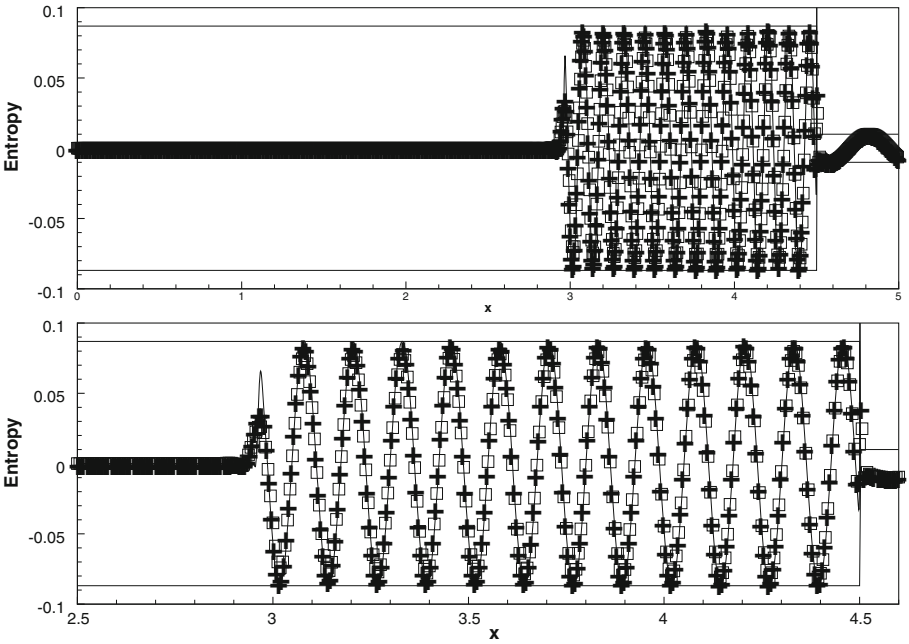

Fig. 10 The shock wave interaction tests. $\kappa = 13$ with 800 points. "*plus*": HWENO, "*square*": WENO. The reference solution is *solid line* and the *zoom* are given in *bottom*

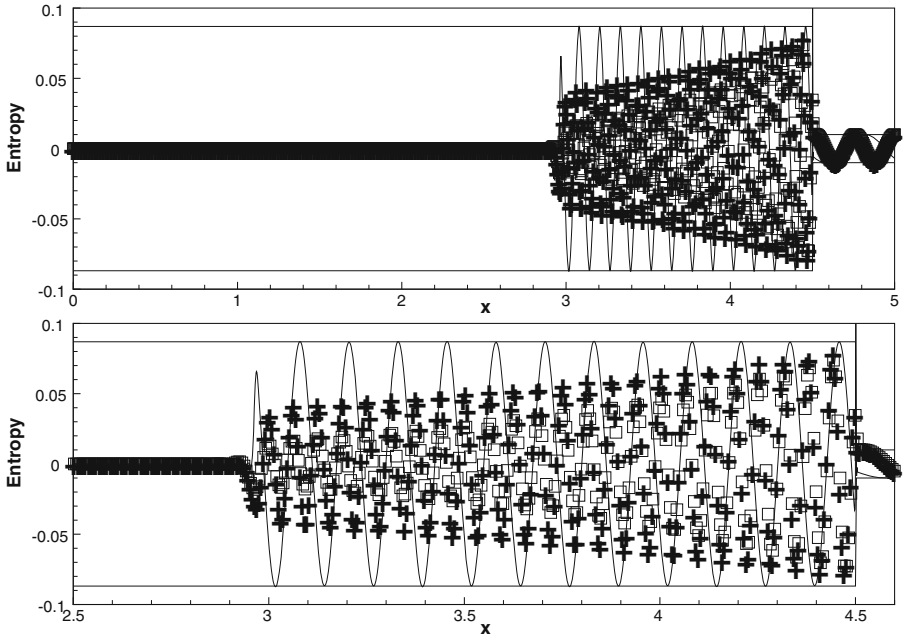

Fig. 11 The shock wave interaction tests. $\kappa = 26$ with 900 points. "*plus*": HWENO, "*square*": WENO. The reference solution is *solid line* and the *zoom* are given in *bottom*

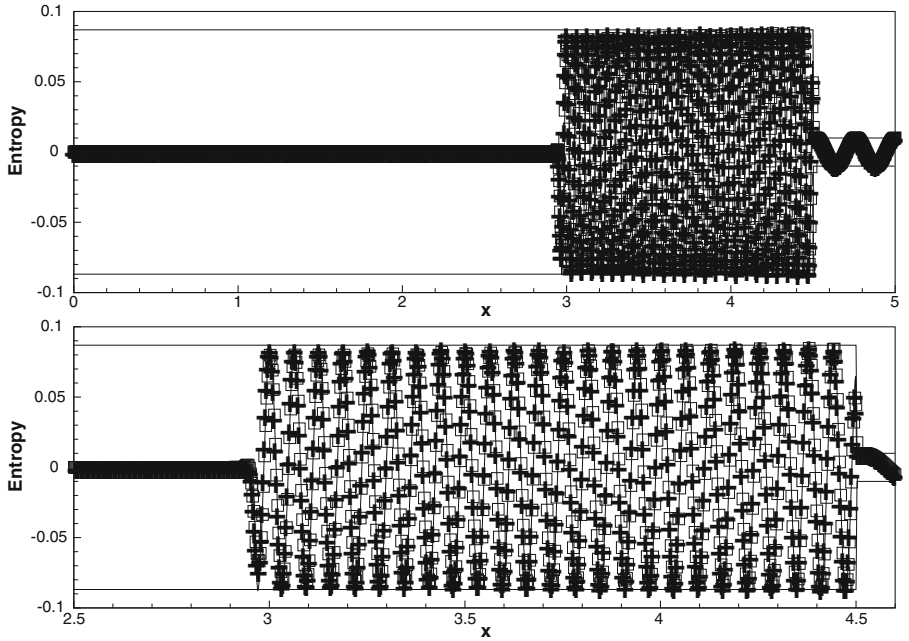

Fig. 12 The shock wave interaction tests. $\kappa = 26$ with 1800 points. "*plus*": HWENO, "*square*": WENO. The reference solution is *solid line* and the *zoom* are given in *bottom*

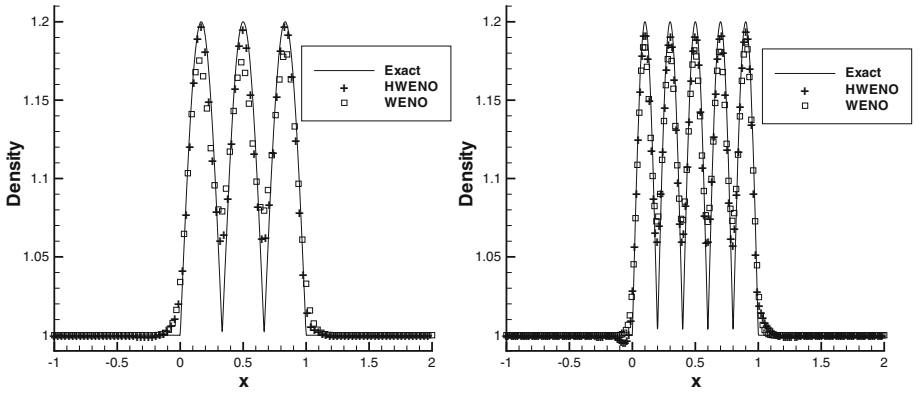

Fig. 13 The moving sine wave tests. $\kappa = 3$ (left) with 100 points, $\kappa = 5$ (*right*) with 200 points. "*plus*": HWENO, "*square*": WENO. The reference solution is *solid line* computed by WENO with 5000 points

$$
\begin{aligned}
u' &= \epsilon\tau e^{\alpha(1-\tau^2)}\sin\theta,\\
v' &= -\epsilon\tau e^{\alpha(1-\tau^2)}\cos\theta,\\
T' &= -\frac{(\gamma-1)\epsilon^2 e^{2\alpha(1-\tau^2)}}{4\alpha\gamma},\\
S' &= 0,
\end{aligned}
$$

where $\tau = r/r_c$, $r = \sqrt{(x-x_0)^2+(y-y_0)^2}$, $\epsilon = 0.3$, $r_c = 0.05$ and $\alpha = 0.204$. Note that here the ϵ, α and r_c indicate the strength , the decay rate and the radius (maximum strength) of the vortex. For more details, one can see [17]. The reflective boundary conditions

Table 4 HWENO spatial discretization schemes, for the two dimensional Burgers' equation $u_t + (u^2/2)_x + (u^2/2)_y = 0$ with initial condition $u_0(x) = 0.5 + \sin((x + y)\pi/2)$, $t = 0.5/\pi$

$Nx \times Ny$	L_1 error	Order	L_2 error	Order	L_∞ error	Order
10×10	6.58E−03		1.32E−02		3.15E−02	
20×20	5.95E−04	3.47	8.86E−04	3.90	2.43E−03	3.69
40×40	1.47E−04	2.02	2.88E−04	1.62	1.07E−03	1.19
80×80	3.05E−05	2.27	1.02E−04	1.50	5.41E−04	0.98
160×160	1.44E−06	4.41	5.99E−06	4.09	4.04E−05	3.74
320×320	1.45E−08	6.63	5.14E−08	6.87	3.05E−07	7.05
640×640	7.13E−10	4.53	1.52E−09	5.12	6.33E−09	5.62

Table 5 The two-dimensional Euler equation. L^1, L^2 and L^∞ errors and numerical order of accuracy by HWENO are measured at the center of each element. Using N equally spaced cells

$Nx \times Ny$	L_1 error	Order	L_2 error	Order	L_∞ error	Order
10×10	1.75E−02		2.01E−02		3.16E−02	
20×20	3.25E−03	2.43	3.86E−03	2.38	7.20E−03	2.13
40×40	2.53E−04	3.69	3.57E−04	3.44	9.00E−04	3.00
80×80	3.62E−06	6.13	5.00E−06	6.16	1.19E−05	6.25
160×160	1.06E−07	5.10	1.20E−07	5.38	1.88E−07	5.98
320×320	6.33E−09	4.06	7.03E−09	4.09	9.97E−09	4.24
640×640	3.95E−10	4.00	4.38E−10	4.00	6.20E−10	4.01

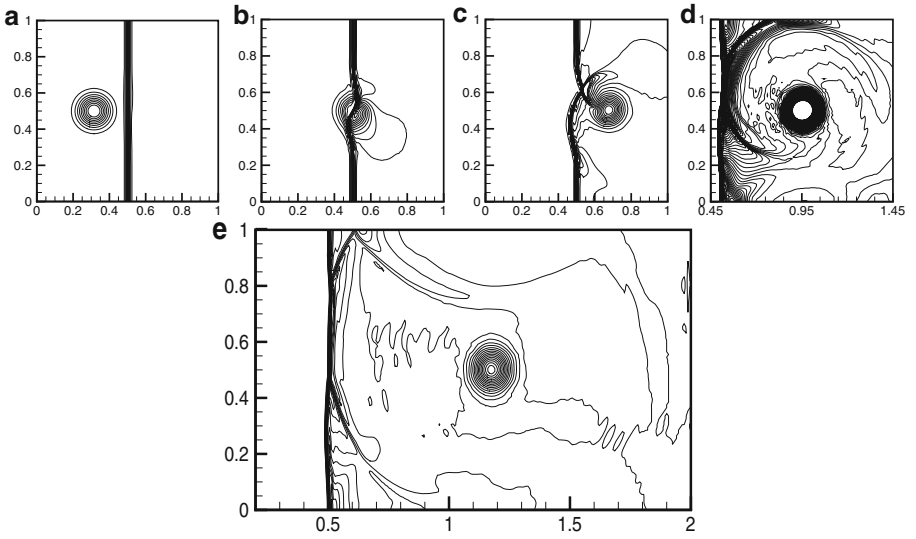

Fig. 14 2D shock vortex interaction

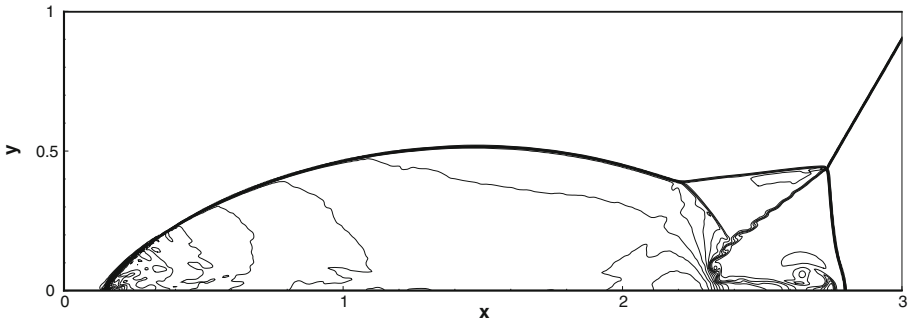

(a) 960×240 meshes

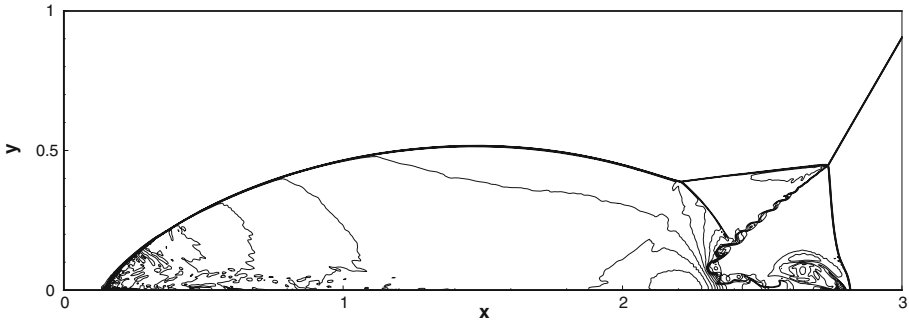

(b) 1920×480 meshes

Fig. 15 Double Mach reflection. 30 equally spaced density contours from 1.5 to 22.7. **a** 960×240 cells, **b** 1920×480 cells

are used at the upper and lower boundaries. The density contours obtained by HWENO at time $t = 0.05,\ t = 0.2,\ t = 0.35,\ t = 0.6$ and $t = 0.8$ in Fig. 14. Comparing the qualitative to [17], we can see that the results show the present HWENO method can attain high accuracy order and capture the vortex and the shock very well.

Example 4.13 Double Mach Reflection.

Double Mach reflection problem: This is again a standard test case for high-resolution schemes. The computational domain for this problem is taken to be $[0, 4] \times [0, 1]$. Consider the reflection of a planar Mach shock in air from a wedge. The setup of a Mach 10 shock which initially makes a 60 degree angle with a reflecting wall (upper left). When the shock hits the sloping wall, a complicated shock reflection occurs. The wave pattern consists of two Mach stems with two contact discontinuities (lower wall). The reflecting wall of wedge lies at the bottom of the computational domain starting from $x = 1/6$. A detailed description of this problem can be found in [14,22]. Figure 15 shows quite pleasing results of the present HWENO scheme with 960×240 and 1280×480 in the computational domain. All the figures show 30 equally spaced density contours from 1.5 to 22.7.

5 Concluding Remarks

In this paper, we present an alternative formulation to reconstruct the numerical fluxes for finite difference Hermite WENO, in which we first use the solution and its derivatives directly to interpolate point values at interfaces of computational cells, then we put the point values at interface of cell in building block to generate numerical fluxes. The building block can be arbitrary monotone fluxes. Comparing with [10], one major advantage is that arbitrary monotone fluxes can be used in this framework, while in [10] the traditional practice of reconstructing flux functions can be applied only to smooth flux splitting. In addition, comparing with classic WENO scheme, one major advantage of HWENO scheme is its compactness in the reconstruction. The numerical errors by HWENO are smaller than WENO schemes under the same grids in our test cases, and numerical results by HWENO scheme are better or comparable to those by WENO scheme for test cases with shock. As in [10], we would also like to point out that HWENO scheme requires more computer memory and CPU time comparing with the original WENO scheme when using the same number of grid points, this is a weak point of HWENO comparing with the original WENO scheme. We have investigated the performance of different numerical fluxes instead of Lax–Friedrichs flux in (2.5) based on the HWENO methods, we observe that the schemes with other flux, such as the LLF flux or HLLC flux, have better performance than the scheme with LF flux. The research of HWENO with different time discretization, such as Lax–Wendroff time discretization is going on.

References

1. Balsara, D.S., Shu, C.-W.: Monotonicity prserving WENO schemes with increasingly high-order of accuracy. J. Comput. Phys. **160**, 405–452 (2000)
2. Capdeville, G.: A new category of Hermitian upwind schemes for computational acoustics. J. Comput. Phys. **210**, 133–170 (2005)
3. Harten, A.: High resolution schemes for hyperbolic conservation laws. J. Comput. Phys. **49**, 357–393 (1983)
4. Harten, A.: Preliminary results on the extension of ENO schemes to two-dimensional problems. In: Proceedings of the International Conference on Hyperbolic Problems, Saint Etienne, January (1986)
5. Harten, A., Engquist, B., Osher, S., Chakravarthy, S.R.: Uniformly high order accurate essentially non-oscillatory schemes, III. J. Comput. Phys. **71**, 231–303 (1987)
6. Hu, C., Shu, C.-W.: Weighted essentially non-oscillatory schemes on triangular meshes. J. Comput. Phys. **150**, 97–127 (1999)
7. Hu, X.Y., Adams, N.A., Shu, C.-W.: Positivity-preserving method for high-order conservative schemes solving compressible Euler equations. J. Comput. Phys. **242**, 169–180 (2013)
8. Jiang, G., Shu, C.-W.: Efficient implementation of weighted ENO schemes. J. Comput. Phys. **126**, 202–228 (1996)
9. Jiang, Y., Shu, C.-W., Zhang, M.P.: An alternative formulation of finite difference weighted ENO schemes with Lax–Wendroff time discretization for conservation laws. SIAM J. Sci. Comput. **35**, A1137–A1160 (2013)
10. Liu, H., Qiu, J.: Finite difference Hermite WENO schemes for conservation laws. J. Sci. Comput. **63**, 548–572 (2015)
11. Liu, X.D., Osher, S., Chan, T.: Weighted essentially non-oscillatory schemes. J. Comput. Phys. **115**, 200–212 (1994)
12. Qiu, J., Shu, C.-W.: Hermite WENO schemes and their application as limiters for Runge–Kutta Galerkin method: one-dimension case. J. Comput. Phys. **193**, 115–135 (2003)
13. Qiu, J., Shu, C.-W.: Finite difference WENO schemes with Lax–Wendroff type time discretizations. SIAM J. Sci. Comput. **24**, 2185–2198 (2003)
14. Qiu, J., Shu, C.-W.: Hermite WENO schemes and their application as limiters for Runge–Kutta discontinuous Galerkin method II: two-dimensional case. Comput. Fluids **34**, 642–663 (2005)

15. Qiu, J., Shu, C.-W.: Hermite WENO schemes for Hamilton–Jacobi equations. J. Comput. Phys. **204**, 82–99 (2005)
16. Shi, J., Hu, C., Shu, C.-W.: A technique of treating negative weights in WENO schemes. J. Comput. Phys. **175**, 108–127 (2002)
17. Shu, C.-W.: Essentially non-oscillatory and weighted essentially non-oscillatory schemes for hyperbolic conservation laws In: Cockburn B., Johnson C., Shu C.-W., Tadmor E., Quarteroni A. (eds.) Advanced Numerical Approximation of Nonlinear Hyperbolic Equations, Lecture Notes in Mathematics, vol. 1697, pp. 325–432. Springer, Berlin (1998)
18. Shu, C.-W.: High order weighted essentially non-oscillatory schemes for convection dominated problems. SIAM Rev. **51**, 82–126 (2009)
19. Shu, C.-W., Osher, S.: Efficient implenmentiation of essentially non-oscillatory shock-capturing schemes. J. Comput. Phys. **77**, 439–471 (1988)
20. Shu, C.-W., Osher, S.: Efficient implenmentiation of essentially non-oscillatory shock-capturing schemes, II. J. Comput. Phys. **83**, 32–78 (1989)
21. Toro, E.F., Spruce, M., Speares, W.: Restoration of the contact surface in the Harten–Lax–van Leer Riemann solver. J. Shock Waves **4**, 25–34 (1994)
22. Woodward, P., Colella, P.: The numerical simulation of two-dimensional fluid flow with strong shocks. J. Comput. Phys. **54**, 115–173 (1984)
23. Zhang, X., Shu, C.-W.: Maximum-principle-satisfying and positivity-preserving high-order schemes for conservation laws: survey and new developments. Proc. R. Soc. A Math. Phys. Eng. Sci. **467**, 2752–2776 (2011)
24. Zhang, X., Shu, C.-W.: Positivity-preserving high order finite difference WENO schemes for compressible Euler equations. J. Comput. Phys. **231**, 2245–2258 (2012)
25. Zhu, J., Qiu, J.: Hermite WENO schemes and their application as limiters for Runge–Kutta discontinuous Galerkin method, III: unstructured meshes. J. Sci. Comput. **39**, 293–321 (2009)
26. Zhu, J., Qiu, J.: WENO schemes and their application as limiters for RKDG methods based on trigonometric approximation spaces. J. Sci. comput. **55**, 606–644 (2013)